Thermodynamic analysis of halide binding to haloalkane dehalogenase suggests the occurrence of large conformational changes

Krooshof, Geja H.; Floris, René; Tepper, Armand W.J.W.; Janssen, Dick B.

Published in:
Protein Science

DOI:
10.1110/ps.8.2.355

Protein Science (1999), *8*:355–360. Cambridge University Press. Printed in the USA.

Thermodynamic analysis of halide binding to haloalkane dehalogenase suggests the occurrence of large conformational changes

GEJA H. KROOSHOF, RENÉ FLORIS, ARMAND W.J.W. TEPPER, AND DICK B. JANSSEN

Department of Biochemistry, Groningen Biomolecular Sciences and Biotechnology Institute, University of Groningen, Nijenborgh 4, 9747 AG Groningen, The Netherlands

(RECEIVED August 14, 1998; ACCEPTED October 14, 1998)

Abstract

Haloalkane dehalogenase (DhlA) hydrolyzes short-chain haloalkanes to produce the corresponding alcohols and halide ions. Release of the halide ion from the active-site cavity can proceed via a two-step and a three-step route, which both contain slow enzyme isomerization steps. Thermodynamic analysis of bromide binding and release showed that the slow unimolecular isomerization steps in the three-step bromide export route have considerably larger transition state enthalpies and entropies than those in the other route. This suggests that the three-step route involves different and perhaps larger conformational changes than the two-step export route. We propose that the three-step halide export route starts with conformational changes that result in a more open configuration of the active site from which the halide ion can readily escape. In addition, we suggest that the two-step route for halide release involves the transfer of the halide ion from the halide-binding site in the cavity to a binding site somewhere at the protein surface, where a so-called collision complex is formed in which the halide ion is only weakly bound. No large structural rearrangements are necessary for this latter process.

Keywords: conformational changes; DhlA; halide binding; haloalkane dehalogenase; pre-steady-state kinetics; thermodynamic analysis

Haloalkane dehalogenase (DhlA) from *Xanthobacter autotrophicus* GJ10 is capable of hydrolyzing short-chain haloalkanes to produce the corresponding alcohols and halide ions. This remarkable ability to cleave carbon-halogen bonds in xenobiotic chemicals makes it an important catalyst in the biotechnological removal of contaminants. X-ray structures of DhlA show that the reaction takes place in a mainly hydrophobic cavity located between two domains: the main domain with an α/β-hydrolase fold structure and the smaller α-helical cap domain lying on top of the main domain (Verschueren et al., 1993a). The active-site cavity is formed by a number of hydrophobic residues, the catalytic triad residues Asp124, His289, and Asp260, and the halide-binding site formed by Trp125 and Trp175.

A kinetic mechanism (Fig. 1) has been formulated for haloalkane dehalogenase on the basis of the catalytic mechanism (Verschueren et al., 1993b; Pries et al., 1994, 1995) and kinetic measurements (Schanstra et al., 1996a; Schanstra & Janssen, 1996). The conversion of 1,2-dibromoethane (DBE), which is the best substrate known for DhlA, starts with DBE entering the active-site cavity ($E \cdot DBE$) followed by a nucleophilic attack of Asp124 on the bromine-carrying C_1 atom of the substrate. This results in the cleavage of the carbon-bromine bond with the concomitant production of a bromoethyl-enzyme intermediate and a bromide ion ($E\text{-}R \cdot Br^-$), the latter of which is bound between the two tryptophans of the halide-binding site. Next, the covalent intermediate is hydrolyzed by a water molecule activated by His289 and Asp260. The 2-bromoethanol molecule that is formed leaves the cavity immediately and the bromide ion remains in the active site ($E \cdot Br^-$). Finally, the bromide ion is exported from the cavity to the solvent,

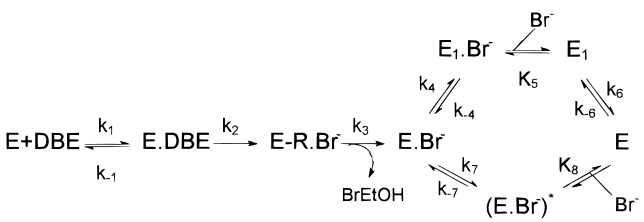

Fig. 1. Schematic representation of the conversion of 1,2-dibromoethane (DBE) by haloalkane dehalogenase. Only kinetically relevant steps are shown.

Reprint requests to: Dick B. Janssen, Department of Biochemistry, University of Groningen, Nijenborgh 4, 9747 AG Groningen, The Netherlands; e-mail: D.B.Janssen@chem.rug.nl.

which happens to be the slowest and most complex process during catalysis.

Kinetic analysis of halide binding and release showed that there are two reversible parallel routes for the bromide ion to leave the active site (Fig. 1; Schanstra & Janssen, 1996). In the first route (upper route in Fig. 1), a slow unimolecular enzyme isomerization process (k_4) leads to an "open" conformation ($E_1 \cdot Br^-$) from which the bromide ion can rapidly dissociate (K_5). After this, the free enzyme reverts to a "closed" state. According to this route, bromide binding starts with a slow conformational change of the free enzyme (k_{-6}), leading to a more "open" form of DhlA (E_1). After rapid binding, the enzyme reverts to a form from which the bromide ion cannot quickly escape (k_{-4}). The second export route for the bromide ion (lower route in Fig. 1) starts with a slow unimolecular step (k_7), which is followed by a fast bimolecular reaction step in which bromide is released (K_8). During the normal catalytic cycle, bromide release mainly proceeds via the upper route, since reaction step k_4 is faster than k_7. The isomerization step (k_4) before bromide release in the upper route is therefore the main rate limiting step during conversion of 1,2-dibromoethane (Schanstra et al., 1996a).

Although the kinetics of bromide binding and release have been studied in detail, little is known about the structural processes associated with the three slow unimolecular steps. It has been suggested that these enzyme isomerization steps involve structural changes in the cap domain, since this part of DhlA is thought to have considerable flexibility (Schanstra et al., 1996b; Schanstra & Janssen, 1996). To learn more about the structural processes and thermodynamic driving forces that are associated with the unimolecular isomerization steps, we have used the Arrhenius equation to derive thermodynamic parameters for these steps by evaluating the temperature dependence of the corresponding rate constants k_4, k_{-6}, k_7, and k_{-7} (Fig. 1). The Van't Hoff equation was used to determine the thermodynamic properties of the overall bromide binding and release.

Results and discussion

Temperature dependence of the steady-state bromide dissociation constant

The steady-state fluorescence after mixing DhlA with various concentrations of bromide was used to calculate the fraction of the total fluorescence that is quenched at saturating bromide concentrations (f_a) and the apparent bromide dissociation constant (K_d). The f_a (0.33) was constant within the temperature range used in the experiments. The affinity of DhlA for bromide ions decreased twofold when the temperature was increased from 15–35 °C (Table 1). The Van't Hoff plot was linear (Fig. 2A), suggesting that the heat capacity change is small. Van't Hoff analysis yielded the thermodynamic parameters in Table 2. The contribution of the entropy to the Gibbs free energy is substantial and positive in the temperature range studied. Therefore, we can conclude that bromide release is entropically driven.

Kinetic and thermodynamic analysis of bromide binding and release at different temperatures

The kinetics of bromide binding and release were studied in the range of 15–40 °C by stopped-flow fluorescence experiments in which enzyme (5 μM) was rapidly mixed with 10–1000 mM NaBr (concentrations after mixing). The fluorescence transients could all be fitted by a single-exponential equation (Fig. 3A), which gave an observed bromide binding rate (k_{obs}) for each bromide concentration. The dependence of k_{obs} on the bromide concentration is shown in Figure 3B for each temperature. These plots all display a typical biphasic behavior. In the first part of the plot, k_{obs} decreases as the bromide concentration increases in the range of 0–20 mM bromide. This is in agreement with a reaction scheme in which isomerization steps have to precede binding and release of the bromide ion (upper route in Fig. 1). In the second part of the plot, k_{obs} increases with increasing bromide concentrations and displays saturation behavior at high bromide concentrations. This hyperbolic

Table 1. *Bromide-dissociation constants and associated rate constants of haloalkane dehalogenase at pH 8.2 and different temperatures*

T (K)	K_d (mM)	k_4 (s^{-1})	k_{-6} (s^{-1})	k_7 (s^{-1})	k_{-7} (s^{-1})	K_8 (M)
288	4.0 ± 0.4	1.0	0.5	0.10	24	0.99
293	4.9 ± 0.3	2.0	0.9	0.16	37	1.01
298	5.0 ± 0.3	3.5	2.1	0.34	60	0.99
303	6.6 ± 0.4	8.6	3.6	0.51	95	1.24
308	7.9 ± 0.3	56	10.1	1.1	200	1.53
313	9.0 ± 1.3	67	22	2.0	310	1.50

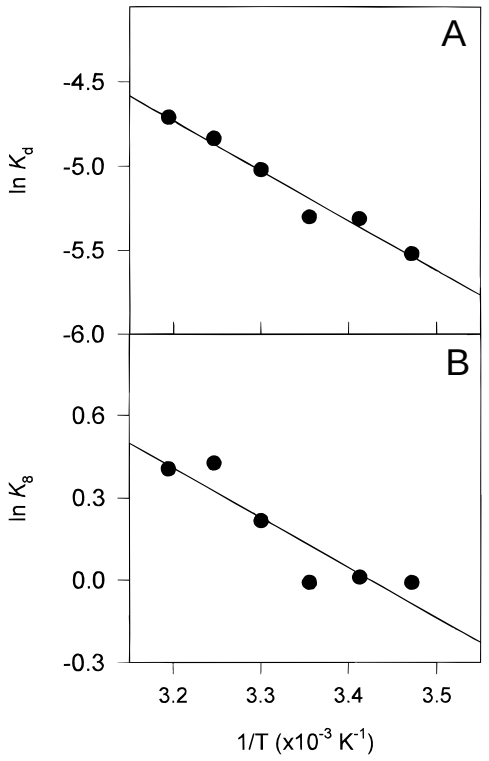

Fig. 2. Van't Hoff analysis of the temperature dependencies of (**A**) the overall steady-state bromide dissociation constant and (**B**) equilibrium constant K_8. The solid lines are linear least-squares fits of the data (see Table 2).

Table 2. *Thermodynamic parameters for overall bromide release from haloalkane dehalogenase obtained from Van't Hoff analysis at pH 8.2 and 30 °C (303 K)*

Reaction step in Figure 1	$\Delta G°$ (kJ mol^{-1})	$\Delta H°$ (kJ mol^{-1})	$\Delta S°$ (J mol^{-1} K^{-1})
Overall Br^- release[a]	12.7	24.6	39.5
Overall Br^- release[b]	12.7	25.4	42.1
K_7 (k_7/k_{-7})[c]	13.2	10.3	−9.5
K_8[d]	−0.5	15.1	51.6

[a] Parameters obtained from Van't Hoff plot (Fig. 2A).
[b] $K_7 + K_8$.
[c] Parameters obtained from Table 3.
[d] Parameters obtained from Van't Hoff plot (Fig. 2B).

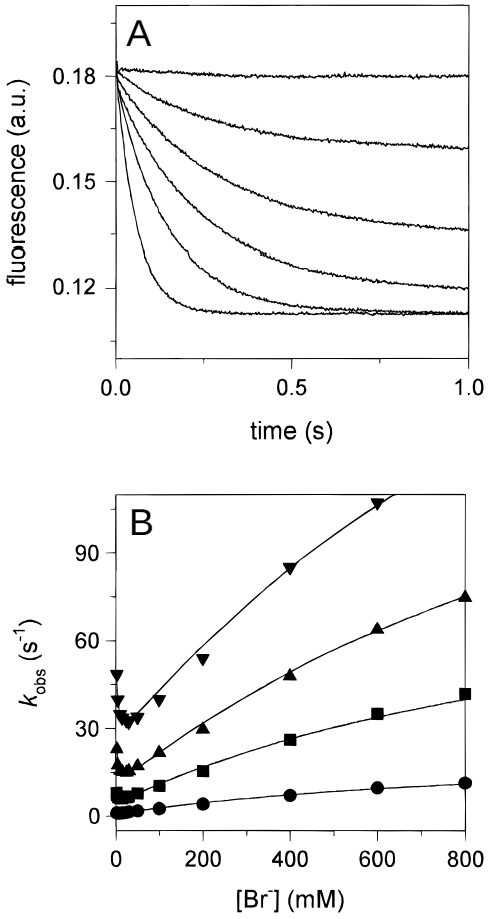

Fig. 3. Kinetics of bromide binding to haloalkane dehalogenase. **A:** Stopped-flow kinetic transients showing the intrinsic tryptophan fluorescence (λ_{ex} = 290 nm, $\lambda_{em} > 320$ nm, arbitrary units) upon mixing 5 μM of enzyme with 0, 2.5, 10, 30, 100, and 400 mM NaBr in T_{50}EMAG buffer at pH 8.2 and 25 °C (end concentrations). All traces are well described by a single-exponential equation with an observed rate constant k_{obs}. **B:** Dependence of the observed rate constant k_{obs} on the bromide concentration over a temperature range of 15–40 °C (288–313 K). The solid lines are fits obtained by simulation of halide binding and release as depicted in the last part of Figure 1.

increase of k_{obs} (20–800 mM bromide) can be explained by assuming a second, parallel binding route involving the rapid formation of a collision complex followed by a slow unimolecular step, as is depicted in the lower route of Figure 1 (Fersht, 1985; Johnson, 1995; Schanstra & Janssen, 1996). Both routes must operate in parallel, since the time course of the fluorescence quenching traces followed single exponentials over the whole concentration range. From the plots of k_{obs} vs. time, rate and equilibrium constants can be obtained using numerical analysis (Schanstra & Janssen, 1996). Since no jump of the fluorescence intensity was observed in the dead time of the instrument, the fluorescence traces can only be simulated by assuming that the fluorescence of the collision complex $(E \cdot Br^-)^*$ is not quenched by the bound bromide ion. This suggests that in this complex the bromide ion is not located between the tryptophan residues in the active-site cavity, but is bound to a binding site somewhere at the protein surface. Unique solutions could be obtained for the unimolecular rate constants k_4, k_{-6}, k_7, and k_{-7}, with an accuracy of ±10% (Table 1). The other reaction steps in the upper route are too fast for accurate measurements, with $k_{-4} > 400$ s^{-1} and $k_6 > (100 * k_{-6})$ at each temperature. The equilibrium constant K_5 depends on the equilibria $E \cdot Br^- \leftrightarrow E_1 \cdot Br^-$ and $E \leftrightarrow E_1$ and could not be determined because only lower limits were obtained for k_{-4} and k_6. For the lower route, the equilibrium constants of both steps could be determined (k_7/k_{-7} and K_8). At each temperature these values were in accordance with the measured overall K_d.

The unimolecular rate constants all increased with increasing temperature. Plotting $\ln k_i$ vs. $1/T$ resulted in Arrhenius plots (Fig. 4) from which the energies of activation ($E_{a,i}$) and pre-exponential factors (A_i) could be determined (Table 3). All four isomerization steps have activation energies (≥80 kJ mol^{-1}) that are typical of reactions involving protein conformational changes (Gutfreund, 1995). All three steps k_4, k_{-6}, and k_7 are associated with enzyme isomerization steps that lead to a form of the enzyme that can rapidly bind or release a bromide ion. Yet, there is a striking difference between the upper and the lower route. The

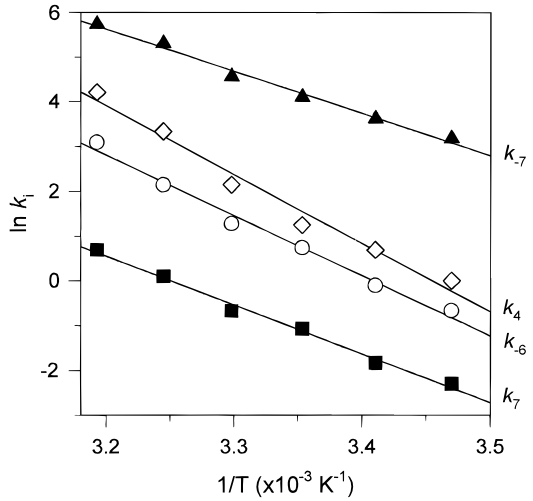

Fig. 4. Arrhenius plot for the unimolecular rate constants involved in the three-step route (open symbols) and two-step route (filled symbols) for bromide export (upper and lower routes in Fig. 1, respectively). The solid lines are the linear least-squares fits of the data.

Table 3. *Thermodynamic parameters of the transition states of the unimolecular steps involved in bromide binding and release in haloalkane dehalogenase at pH 8.2 and 30 °C (303 K)*

Reaction step in Figure 1	$E_a^{\ddagger}$ (kJ mol^{-1})	$\Delta H^{\ddagger}$ (kJ mol^{-1})	$\Delta G^{\ddagger}$ (kJ mol^{-1})	$\Delta S^{\ddagger}$ (J mol^{-1} K^{-1})	log A_{extrap}[a]	log A_{calc}[b]
$E\cdot Br^- \rightarrow E_1\cdot Br^-$ (k_4)	129 ± 9.5	126 ± 9.5	68.8 ± 0.3	190	23.0 ± 0.1	23.1
$E \rightarrow E_1$ (k_{-6})	114 ± 5.8	111 ± 5.8	71.0 ± 0.3	135	20.1 ± 0.1	20.3
$E\cdot Br^- \rightarrow (E\cdot Br^-)^*$ (k_7)	88.6 ± 4.3	86.1 ± 4.3	75.9 ± 0.3	33.5	15.4 ± 0.1	15.0
$(E\cdot Br^-)^* \rightarrow E\cdot Br^-$ (k_{-7})	78.3 ± 4.0	75.8 ± 4.0	62.8 ± 0.3	43.0	15.5 ± 0.1	15.5

[a]Obtained from Arrhenius plot by extrapolation to $T \rightarrow \infty$.
[b]Calculated from $\Delta S^{\ddagger}$.

slow unimolecular steps k_4 and k_{-6} of the upper route of Figure 1 have higher activation energies than step k_7 in the lower route, though they are 20- and 8-fold faster than step k_7, respectively. The structural changes associated with the isomerization steps in the upper route must therefore be different from those taking place in the lower route. Also step k_{-7} has a lower activation energy than k_4 and k_{-6} in the upper route.

The pre-exponential factors (A) associated with steps k_4 and k_{-6} are also very high as compared to the other steps in the reaction mechanism (Table 3). In fact, the pre-exponential terms of 10^{23} and 10^{20} for step k_4 and k_{-6}, respectively, exceed the limit of simple molecular rotations and vibrations ($\sim 10^{14}$) by multiple orders of magnitude and therefore cannot be interpreted in terms of meaningful frequency factors (Gutfreund, 1995; Fitzgerald et al., 1996). This could provide evidence that large-scale protein motions involving many bond torsions may occur in reaction steps k_4 and k_{-6}. Similar pre-exponential factors of 10^{24}–10^{25} were found by Fitzgerald et al. (1996) when studying a hinged loop rearrangement near a buried artificial cavity in cytochrome *c* peroxidase.

The values of $E_{a,i}$ and A_i, together with the rate constants (k_i), were used to calculate the free energies of activation ($\Delta G^{\ddagger}$), enthalpies of activation ($\Delta H^{\ddagger}$), and entropies of activation ($\Delta S^{\ddagger}$) (Table 3). The difference in the magnitudes of the activation free energies for the four reaction steps reflects the difference in rate constants: the slowest step, $E\cdot Br^- \rightarrow (E\cdot Br^-)^*$ has the highest value for $\Delta G^{\ddagger}$. Furthermore, the entropic and enthalpic contributions to the free energies of activation are negative and positive, respectively, for all four isomerizations. The pre-exponential factors were also calculated from the activation entropy (Equation 8) and proved to be nearly identical to the A values determined by extrapolation of the Arrhenius plots (Table 3). Since both the forward and reverse reaction rates, k_7 and k_{-7}, could be determined, we could calculate the standard free energy, reaction enthalpy, and entropy for this reversible unimolecular step (Table 2). Together with the thermodynamic parameters of K_8, which were obtained from Van't Hoff analysis (Fig. 2B), we could calculate the standard thermodynamic parameters of overall halide release, which were in good agreement with the values obtained directly from Van't Hoff analysis of the overall K_d (Table 2).

Interestingly, both transitions k_4 and k_{-6} in the upper route of Figure 1 have significantly larger transition state entropies and enthalpies compared with the values of the isomerization steps k_7 and k_{-7} in the lower route (see Table 3). Thus, the entropy components are much more important in the transition state free energies of the unimolecular steps in the upper route than in the lower route.

The large activation entropies for steps k_4 and k_{-6} are indicative of considerable structural rearrangements. It has been suggested that bromide release may require the entrance of water molecules into the active-site cavity (Schanstra & Janssen, 1996). A large entropy effect can be expected both because of structural changes and desolvation processes (Rand, 1992; Gutfreund, 1995). A transition state in which the halide ion is both bound to the protein and solvated is difficult to envision without significant structural changes, since the buried active-site cavity is too small to accommodate both a halide ion and a number of water molecules. Furthermore, the transition states of steps k_4 and k_{-6} show similar entropy and enthalpy contributions although no halide is present during the process described by k_{-6}. The isomerization observed in the upper route could involve significant conformational changes leading to a more open structure and the formation of a solvent accessible channel that leads to the active site. Similar changes were observed in cytochrome *c* peroxidase (Fitzgerald et al., 1996).

The activation enthalpies associated with all four unimolecular steps are consistent with disruption of multiple interactions, which can be Van der Waals interactions, hydrogen bonds or ion pairs, individually corresponding to energies in the range of 1–10, 12–25, and 20–50 kJ mol^{-1}, respectively (Fersht, 1985). The activation enthalpies of 126 and 111 kJ mol^{-1} for reaction steps k_4 and k_{-6}, respectively, are relatively high and may even reflect the cis-trans isomerization of a proline residue, the activation enthalpy of which lies in the range of 92–113 kJ mol^{-1} (Koide et al., 1993; Fitzgerald et al., 1996; Veeraraghavan et al., 1997). Proline cis-trans isomerization could serve as a hinge point in the movement of a loop or flap to open a cavity for the entry of ligands as observed in *Candida rugosa* lipase (Grochulski et al., 1994) and cytochrome *c* peroxidase (Fitzgerald et al., 1996). In haloalkane dehalogenase, Pro57 and Pro168 exist in the cis configuration and they are located in the main and cap domain, respectively (Verschueren et al., 1993a). Pro168 might be the most likely candidate to undergo a cis-trans isomerization during the conformational change, since it is located in an N-terminal helix-loop-helix structure (residues 159–181) in the cap domain that was proposed to be involved in the enzyme isomerization (Schanstra et al., 1996b; Krooshof et al., 1998).

On the basis of the observations mentioned above, we propose that the three-step halide export route (upper route in Fig. 1) involves conformational changes that result in a water accessible active site, which allows solvation and subsequent escape of the halide ion. We suggest that the two-step route (lower route) for halide release involves the transfer of the halide ion from the halide-binding site in the cavity to a binding site somewhere at the

protein surface, where a so-called collision complex is formed in which the halide is only weakly bound. No large structural rearrangements seem to be necessary for this process, but its rate is much lower than that of the upper route (Fig. 1).

Materials and methods

Protein expression and purification

Haloalkane dehalogenase was purified from *Escherichia coli* strain BL21(DE3) transformed with plasmid pGELAF+, which carries the haloalkane dehalogenase gene (*dhlA*) under the control of the T7 promoter (Schanstra et al., 1993). Expression and purification were achieved as described earlier (Schanstra et al., 1993). The enzyme was concentrated with an Amicon ultrafiltration cell using a PM30 filter and stored at −20 or 4 °C in TEMAG buffer (10 mM Tris-sulfate pH 7.5, 1 mM EDTA, 1 mM 2-mercaptoethanol, 3 mM sodium azide, and 10% (v/v) glycerol). Protein concentrations were determined from absorbance measurements at 280 nM, using the absorbance coefficient of $4.87 \times 10^4\ M^{-1}\ cm^{-1}$, and the purity was checked by SDS-polyacrylamide gel electrophoresis.

Halide binding experiments

The pre-steady-state kinetics of halide binding were determined by stopped-flow fluorescence quenching experiments using an Applied Photophysics SX17MV stopped-flow instrument. A wavelength of 290 nM was used for excitation. Equal volumes of the protein and ligand were rapidly mixed and the resultant quenching of the intrinsic protein fluorescence was followed by measuring the fluorescence signal above 320 nm using a cutoff filter. All reactions were performed over a temperature range of 15–40 °C (288–313 K) in TEMAG buffer at pH 8.2. The reported reactant concentrations are those present in the reaction chamber, after mixing. At temperatures higher than 30 °C, fresh enzyme was used for each measurement, which was allowed to equilibrate for a short period of time (max 2 min) to prevent thermal denaturation. All fluorescence traces, which were the average of three individual experiments, were fitted using computer software provided with the stopped-flow instrument.

The apparent halide dissociation constants (K_d) were derived from the steady-state part of the fluorescence traces using nonlinear regression fitting (SigmaPlot, Jandel Scientific) of

$$\frac{(F_0 - F)}{F_0} = \frac{f_a \cdot [X^-]}{[X^-] + K_d} \tag{1}$$

where F is the observed steady-state fluorescence at halide concentration $[X^-]$, K_d is the apparent dissociation constant, and f_a is the fraction of the total fluorescence that is quenched at saturating halide concentrations ($\gg K_d$).

Kinetic data from the pre-steady-state part of the stopped-flow traces were further analyzed by iterative numerical integration, as described previously (Schanstra & Janssen, 1996) using the simulation software Gepasi (Mendes, 1993) linked to the spreadsheet program Quattro-Pro (Borland International Inc.). The Gepasi program uses numerical integration to simulate reaction schemes. The total fluorescence of all enzyme species at each time point was calculated in Quattro-Pro, using a one-third reduction of fluorescence by halide binding. As a constraint in the simulation and fitting process, the dissociation constant for halide binding was used according to

$$K_d = \frac{K_4 k_3 k_{-5}(k_1 + k_{-1})}{k_{-1}(k_3 k_5 + k_{-3} k_5 + k_3 k_{-5})}. \tag{2}$$

Determination of thermodynamic parameters of bromide binding and release

Thermodynamic parameters of bromide binding and release were derived from the temperature dependence of the steady-state bromide dissociation constant using the Van't Hoff equation:

$$\frac{d \ln K_d}{d(1/T)} = -\frac{\Delta H^\circ}{R} \tag{3}$$

where K_d is the apparent bromide dissociation constant, R is the gas constant, T the absolute temperature, and ΔH° is the standard reaction enthalpy. Consequently, a straight line is to be expected with a slope equal to $-\Delta H^\circ/R$ when $\ln K_d$ is plotted against $1/T$.

The dissociation constant was also used to calculate the standard free energy of reaction by

$$\Delta G^\circ = -RT \cdot \ln K_d. \tag{4}$$

Finally, the standard reaction entropy (ΔS°) arises from:

$$\Delta S^\circ = \frac{(\Delta H^\circ - \Delta G^\circ)}{T}. \tag{5}$$

Determination of thermodynamic parameters of activation

Thermodynamic parameters of activation were obtained from the temperature dependence of an elementary reaction rate constant. The energy of activation ($E_{a,i}$) is defined as

$$E_{a,i} = RT^2 \frac{d \ln k_i}{dT}, \tag{6}$$

where R is the gas constant, T the absolute temperature, and k_i the rate constant of reaction step i. Integration of Equation 6 yields

$$\ln k_i = \ln A - \frac{E_{a,i}}{RT}. \tag{7}$$

Both $E_{a,i}$ and A can be considered constant over a temperature range of about 50 K (Chang, 1981), so that plotting $\ln k_i$ vs. $1/T$ results in a linear relationship (Arrhenius plot) with slope $-E_{a,i}/R$ and intercept $\ln A$, to be determined by extrapolation to $T \to \infty$. The pre-exponential factor A may alternatively be calculated by

$$A = \left(\frac{k_B T}{h}\right) \cdot e \left(1 + \frac{\Delta S_i^\ddagger}{R}\right) \tag{8}$$

where k_B is the Boltzmann constant, h is Planck's constant, and $\Delta S_i^\ddagger$ is the transition state entropy belonging to reaction step i.

The free energy of activation ($\Delta G_i^{\ddagger}$), enthalpy of activation ($\Delta H_i^{\ddagger}$), and entropy of activation ($\Delta S_i^{\ddagger}$) for an elementary reaction at a given temperature were subsequently calculated from

$$\Delta G_i^{\ddagger} = RT \cdot \ln\left(\frac{k_B T}{h k_i}\right), \quad (9)$$

$$\Delta H_i^{\ddagger} = E_{a,i} - RT, \quad (10)$$

and

$$\Delta S_i^{\ddagger} = \frac{(\Delta H_i^{\ddagger} - \Delta G_i^{\ddagger})}{T}. \quad (11)$$

References

Chang R. 1981. *Physical chemistry with applications to biological systems*. New York: Macmillan.

Fersht AR. 1985. *Enzyme structure and mechanism*. New York: Freeman.

Fitzgerald MM, Musah RA, McRee DE, Goodin DB. 1996. A ligand-gated, hinged loop rearrangement opens a channel to a buried artificial protein cavity. *Nature Struct Biol 3*:626–631.

Grochulski P, Li Y, Schrag JD, Cygler M. 1994. Two conformational states of *Candida rugosa* lipase. *Protein Sci 3*:82–91.

Gutfreund H. 1995. *Kinetics for the life sciences: Receptors, transmitters and catalysts*. Cambridge, United Kingdom: Cambridge University Press.

Johnson KA. 1995. Rapid quench kinetic analysis of polymerases, adenosinetriphosphatases, and enzyme intermediates. *Methods Enzymol 249*:38–61.

Koide S, Dyson HJ, Wright PE. 1993. Characterization of a folding intermediate of apoplastocyanin trapped by proline isomerization. *Biochemistry 32*:12299–12310.

Krooshof GH, Ridder IS, Tepper AWJW, Vos GJ, Rozeboom HJ, Kalk KH, Dijkstra BW, Janssen DB. 1998. Kinetic analysis and X-ray structure of haloalkane dehalogenase with a modified halide-binding site. *Biochemistry 27*:15013–15023.

Mendes P. 1993. Gepasi: A software package for modeling the dynamics, steady states and control of biochemical and other systems. *Comput Appl Biosci 9*:563–571.

Pries F, Kingma J, Krooshof GH, Jeronimus-Stratingh CM, Bruins AP, Janssen DB. 1995. Histidine 289 is essential for hydrolysis of the alkyl-enzyme intermediate of haloalkane dehalogenase. *J Biol Chem 270*:10405–10411.

Pries F, Kingma J, Pentenga M, van Pouderoyen G, Jeronimus-Stratingh CM, Bruins AP, Janssen DB. 1994. Site-directed mutagenesis and oxygen isotope incorporation studies of the nucleophilic aspartate of haloalkane dehalogenase. *Biochemistry 33*:1242–1247.

Rand RP. 1992. Raising water to new heights. *Science 256*:618.

Schanstra JP, Janssen DB. 1996. Kinetics of halide release of haloalkane dehalogenase: Evidence for a slow conformational change. *Biochemistry 35*:5624–5632.

Schanstra JP, Kingma J, Janssen DB. 1996a. Specificity and kinetics of haloalkane dehalogenase. *J Biol Chem 271*:14747–14753.

Schanstra JP, Ridder IS, Heimeriks GJ, Rink R, Poelarends GJ, Kalk KH, Dijkstra BW, Janssen DB. 1996b. Kinetic characterization and X-ray structure of a mutant of haloalkane dehalogenase with higher catalytic activity and modified substrate range. *Biochemistry 35*:13186–13195.

Schanstra JP, Rink R, Pries F, Janssen DB. 1993. Construction of an expression and site-directed mutagenesis system of haloalkane dehalogenase in *Escherichia coli*. *Protein Expr Purif 4*:479–489.

Veeraraghavan S, Nall BT, Fink AL. 1997. Effect of prolyl isomerase on the folding reactions of staphylococcal nuclease. *Biochemistry 36*:15134–15139.

Verschueren KHG, Franken SM, Rozeboom HJ, Kalk KH, Dijkstra BW. 1993a. Refined X-ray structures of haloalkane dehalogenase at pH 6.2 and pH 8.2 and implications for the reaction mechanism. *J Mol Biol 232*:856–872.

Verschueren KHG, Seljée F, Rozeboom HJ, Kalk KH, Dijkstra BW. 1993b. Crystallographic analysis of the catalytic mechanism of haloalkane dehalogenase. *Nature 363*:693–698.